Localization microscopy coming of age: from concepts to biological impact

Markus Sauer

Department of Biotechnology and Biophysics, Julius-Maximilians-University Würzburg, Am Hubland, 97074 Würzburg, Germany

m.sauerr@uni-wuerzburg.de

Journal of Cell Science 126, 3505–3513
© 2013. Published by The Company of Biologists Ltd
doi: 10.1242/jcs.123612

Summary

Super-resolution fluorescence imaging by single-molecule photoactivation or photoswitching and position determination (localization microscopy) has the potential to fundamentally revolutionize our understanding of how cellular function is encoded at the molecular level. Among all powerful, high-resolution imaging techniques introduced in recent years, localization microscopy excels because it delivers single-molecule information about molecular distributions, even giving absolute numbers of proteins present in subcellular compartments. This provides insight into biological systems at a molecular level that can yield direct experimental feedback for modeling the complexity of biological interactions. In addition, efficient new labeling methods and strategies to improve localization are emerging that promise to achieve true molecular resolution. This raises localization microscopy as a powerful complementary method for correlative light and electron microscopy experiments.

Key words: Super-resolution fluorescence imaging, Localization microscopy, Quantitative imaging, Single-molecule fluorescence detection

Introduction

It is commonly accepted that the emission of a single fluorescent entity, for example, an organic fluorophore, a fluorescent protein or a semiconductor nanocrystal, shows random interruptions of fluorescence emission as a direct consequence of the observation of a single quantum system with discrete states (Dickson et al., 1997; Moerner and Orrit, 1999; Tinnefeld and Sauer, 2005). Ultimately, the finding that not only differences in spectroscopic characteristics such as fluorescence emission wavelength and the lifetime of individual fluorophores (Heilemann et al., 2002; Lacoste et al., 2000; Pertsinidis et al., 2010), but also the temporal emission characteristics (i.e. deterministic or stochastic switching of fluorophores between a fluorescent on-state and a non-fluorescent off-state by means of light) paved the way to resolve the distance between multiple fluorophores separated by less than half the wavelength of light ($<\lambda/2$) (Abbe, 1873; Lidke et al., 2005; Hell, 2007; Galbraith and Galbraith, 2011). Thus, photoswitching, photoactivation or photoconversion of fluorophores attached to the structure of interest in combination with precise single-molecule localization and image reconstruction is the key to bypassing the so-called diffraction barrier and allows us insight into structural details at a resolution that is unmatched so far. As the localization precision (i.e. the accuracy of position determination of a single fluorophore by fitting its emission pattern with a model function) depends mainly on the number of collected photons, N, and on the standard deviation, σ, of the spatial response function of the imaging system to an infinitely small object [the point spread function (PSF)], single fluorophores can be localized with an accuracy that is approximated by $\sigma/N^{1/2}$ for negligible background (Mortensen et al., 2010; Thompson et al., 2002). That is, the detection of only a few thousand photons from a single fluorophore allows the localization of the fluorophore with nanometer precision (Yildiz and Selvin, 2005).

Therefore, it was the discovery of photoconvertible and photoactivatable fluorescent proteins (Patterson and Lippincott-Schwartz, 2002; Ando et al., 2002; Lippincott-Schwartz and Patterson, 2009) and photoswitchable organic fluorophores (Heilemann et al., 2005; Bates et al., 2005) that ultimately cleared the way for localization microscopy. As a logical consequence, photoactivated localization microscopy (PALM) (Betzig et al., 2006; Shroff et al., 2007; Shroff et al., 2008), fluorescence photoactivation localization microscopy (FPALM) (Hess et al., 2006; Hess et al., 2007) and stochastic optical reconstruction microscopy (STORM) using special pairs of fluorophores (Rust et al., 2006; Bates et al., 2007) were introduced shortly afterwards. A short time later, the use of commercially available organic fluorescent probes, such as fluorophore-labeled antibodies or phalloidin probes, was demonstrated for super-resolution imaging by direct STORM (*d*STORM), facilitating the acceptance and broad applicability of localization microscopy (Heilemann et al., 2008; Heilemann et al., 2009; van de Linde et al., 2011a; Jones et al., 2011; Dempsey et al., 2011; Sillibourne et al., 2011; Williamson et al., 2011; Kaminski-Schierle et al., 2011; van de Linde et al., 2012; Zessin et al., 2012; Lampe et al., 2012; Wilmes et al., 2012; Rossy et al., 2013; Mattila et al., 2013). Furthermore, other localization microscopy methods using photoswitching of standard organic fluorophores under slightly different experimental conditions emerged under the names of GSDIM (ground-state depletion microscopy followed by individual molecule return) (Fölling et al., 2008) and blink microscopy (Steinhauer et al., 2008). Transient binding of fluorescent probes to the target structure (Sharonov and Hochstrasser, 2006; Giannone et al., 2010) or the conversion of fluorogenic probes by catalysts (Roeffaers et al., 2009) were also exploited successfully to reconstruct super-resolution fluorescence images.

Journal of Cell Science

This Commentary summarizes the basic requirements of localization microscopy, underscoring the role of single-molecule detection using standard fluorescent probes and discusses its far-reaching prospects. I point out current hurdles that must be overcome to exploit the full potential of localization microscopy and to provide meaningful and possibly quantitative information. The discussion also includes the necessity of efficient labeling strategies (Box 1) and suited reference structures (Box 2) to successfully utilize the full potential of localization microcopy. Finally, I discuss ways of further enhancing the localization precision for individual fluorophores, such as cooling the sample to cryogenic temperatures or the application of elaborate chemical redox cocktails.

Basic principles and artifacts of localization microscopy

Localization microscopy is comparatively easy to implement as it requires only a wide-field microscope equipped with a continuous wave laser with a power of ~100 mW for efficient excitation, a 405 nm laser for activation and a charge-coupled device (CCD) camera for sensitive detection of fluorescence. Together with the availability of efficient open-source software for two-dimensional (2D) and three-dimensional (3D) multicolor localization microscopy (e.g. rapi*d*STORM) (Wolter et al., 2010; Wolter et al., 2012), localization microscopy provides the best cost–benefit ratio among the different super-resolution imaging methods. Furthermore, manufacturers are now offering user-friendly, fully integrated instruments such as N-STORM (Nikon), Elyra PAL-M (Zeiss) and SR GSD (Leica).

When performing localization microscopy, the protein of interest has to be labeled with photoswitchable or photoactivatable fluorophores, the majority of which must be transferred to a non-fluorescent off-state. In the case of photoactivatable fluorophores, the fluorophores essentially reside in their non-fluorescent state before activation. If standard organic fluorophores are used, the majority of fluorophores are converted to a metastable dark state upon irradiation with light. Then, during the experiment, only a stochastic subset of single fluorophores is switched on for a given observation time (e.g. upon irradiation with UV light at 405 nm) and localized. This cycle of photoactivation of fluorescent probes and subsequent readout is repeated to record a stack of thousands of images and reconstruct a super-resolution image from, typically, several tens of thousands to millions of localizations (Fig. 1).

It is important to consider that the extractable structural information from localization microscopy data is not only determined by the optical resolution of the instrument but, equally, by the labeling density. According to information theory, the required density of fluorescent probes has to be sufficiently high to satisfy the Nyquist–Shannon sampling theorem (Shannon,

Box 1. Different sizes of fluorescent labels

- Green fluorescent protein (GFP) is a protein comprising 238 amino acid residues (2–5 nm, 27 kDa), which exhibits bright green fluorescence when exposed to light in the blue to ultraviolet range (Tsien, 1998; Ormö et al., 1996).
- Immunoglobulin G (IgG) antibodies are large molecules (~10 nm, 150 kDa) comprising four peptide chains. IgGs are commonly used in immunocytochemistry applications to target specific peptide or protein antigens in cells (Weber et al., 1978).
- The SNAP-tag uses the human DNA repair enzyme O6-alkylguanine-DNA alkyltransferase (AGT). AGT has a mass of 20 kDa and, in a similar manner to fluorescent proteins, is genetically attached to a protein of interest (Gautier et al., 2008). Labeling is achieved by using fluorophore-labeled O6-benzylguanine substrates that are processed by AGT, which first cleaves off the O6-benzylguanine unit and then covalently binds the fluorophore.
- Phalloidin, a toxin from the death cap (*Amanita phalloides*), binds F-actin and prevents its depolymerization. The bi-cyclic heptapeptide has a molecular mass of 789 g/mol and is approximately four times smaller than GFP and AGT.
- The 1,2,3-triazole linkage (click chemistry) between a fluorophore modified as an azide and a reaction partner (e.g. protein) modified as an alkyne, or vice versa, is extremely stable. Classic click reactions comprise a copper-catalyzed azide–alkyne cycloaddition to label molecules of interest. To avoid cytotoxic effects of Cu(I) DIBO (dibenzycyclooctyne), fluorophore derivatives have been developed (Laughlin et al., 2008). The strain in the eight-membered ring allows the reaction with azide-modified molecules in the absence of Cu(I).

See figure for the different structures.

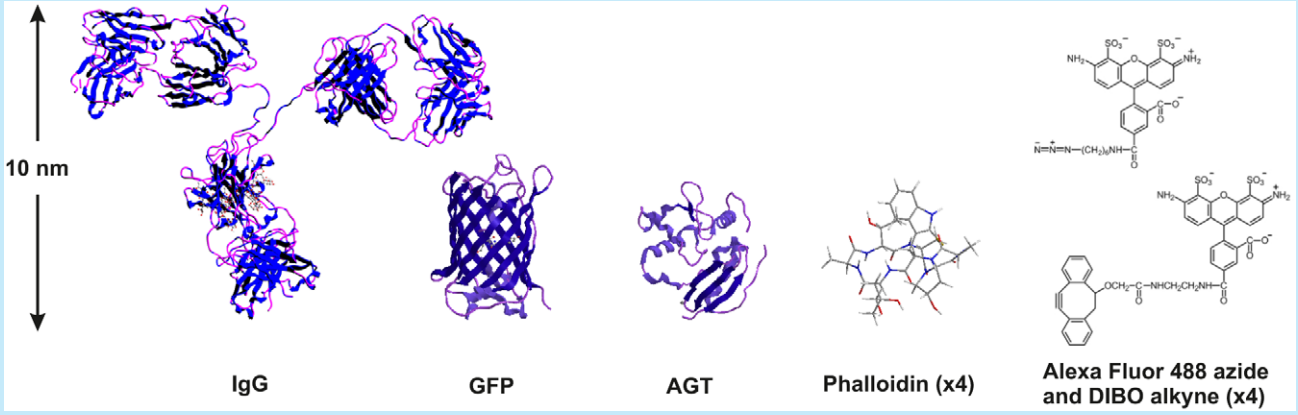

Journal of Cell Science

Box 2. Reference structures for super-resolution imaging

The nuclear core complex (NPC) comprises multiple copies of nucleoporins and represents one of the largest molecular machines in the cell (~120 MDa in the higher eukaryotes). NPCs are wheel-shaped, eightfold symmetrical cylindrical assemblies with an ~125 nm diameter core structure and a height of ~70 nm. They contain eight spokes arranged in a radially symmetrical fashion and a central channel with a diameter of 35–50 nm, as well as a cytoplasmic ring and a nuclear ring (Beck et al., 2007).

Centrosomes, the main microtubule-organizing center (MTOC) possess, in animals, two orthogonally arranged centrioles surrounded by an amorphous mass of pericentriolar material. Each centriole is made up of a ring of nine groups of microtubules with a length of 700 nm and a diameter of 250 nm. The two centrioles are arranged such that one is perpendicular to the other (Kitagawa et al., 2011).

The space separating a presynaptic and postsynaptic cell in a chemical synapse, across which the neurotransmitters have to diffuse for signal transduction, is called the synaptic cleft. Electron micrographs suggest a relatively constant average distance between pre- and postsynaptic membranes, ranging between 15 and 25 nm (Ribrault et al., 2011). That is, dependent on their respective function, pre- and postsynaptic proteins are separated at distances well below the diffraction barrier.

Taking advantage of the self-recognition properties of DNA, rigid, branched DNA motifs based on the complementary Watson–Crick base pairing between segments of a given set of oligonucleotides can be used as a super-resolution imaging ruler. The DNA origami method introduced by Rothemund in 2006 (Rothemund, 2006) folds a long single-stranded DNA strand (scaffold) into a desired 2D or 3D shape with the help of hundreds of short oligonucleotides, called staple strands. Because fluorophores can be attached to staple strands or hybridized through a complementary DNA strand, DNA origami allows the synthesis of identical nanostructures in a single experiment (Tørring et al., 2011; Saccà and Niemeyer, 2012).

1949). In essence, the theorem states that the mean distance between neighboring localized fluorophores (the sampling interval) must be at least twice as fine as the desired resolution. For example, to resolve 20 nm structural features in one dimension, a fluorophore must be localized at least every 10 nm. In order to allow the isolated localization of individual fluorophores, only one fluorophore out of all fluorophores present within the diffraction-limited area, accounting for a specific structure, is allowed to reside in its fluorescent state at any time during the experiment (Fig. 1A–D). This implies that the lifetime of the off-state has to be substantially longer than the lifetime of the on-state or, in other words, the photoswitching ratio $r=k_{off}/k_{on}$ must be high enough to minimize false multiple-fluorophore localizations (van de Linde et al., 2010) (Fig. 1E–H). If the fluorophores are arranged along a single filament, false localizations have no impact on the structural resolution perpendicular to filament extension. In the case of two adjacent fluorophores on crossing filaments, the generation of a false localization will affect the ability to resolve both filaments independently. Consequently, false localizations owing to inappropriate photoswitching rates or fluorophore densities that are too high can give rise to the appearance of fluorophore clusters instead of revealing, for example, crossing cytoskeletal filaments that are possibly loaded with cargo vesicles (Fig. 1E–H).

It must be pointed out that, in practice, the density of fluorescent spots should be well below one emitter per μm^2 to enable reliable spot finding and fitting (Wolter et al., 2011). If, for any reason, the emitter density increases (e.g. to increase the temporal resolution in live-cell experiments), the number of erroneously analyzed overlapping PSFs increases as well. These localization errors are included as artifacts in the reconstructed super-resolution image and can lead to unresolved features and misinterpretation. Here, new approaches such as DAOSTORM (Holden et al., 2011) and compressed sensing (Zhu et al., 2012) promise to put things right, allowing a fluorophore density of up to 10 emitters per μm^2 with tolerable error rates.

Efficient fluorescence labeling

Because the density of fluorophores controls the achievable structural resolution (Shannon, 1949), efficient and specific labeling with fluorescent probes is another decisive aspect of super-resolution imaging. Photoactivatable fluorescent proteins, such as EosFP, psCFP, PAGFP, PAmCherry and PAtagRFP are undoubtedly the labels of choice for live-cell localization microscopy because they can be genetically fused to the protein of interest (Betzig et al., 2006; Hess et al., 2007; Shroff et al., 2007; Manley et al., 2008; Shroff et al., 2008; Subach et al., 2009). Thus, in the ideal case, each protein carries a single fluorophore and shows wild-type functionality. With a molecular mass of ~27 kDa, a barrel-like structure and a size of 2–5 nm (Tsien, 1998; Ormö et al., 1996) (Box 1), a fluorescent protein can, however, perturb protein functionality. Furthermore, besides a few exceptions, such as farnesylated Eos fused to the plasma membrane marker CAAX (Kanchanawong et al., 2010), fluorescent proteins do not have a direct extension to other classes of biomolecules, including lipids, nucleic acids, glycans and secondary metabolites, and have less-than-optimal fluorescent properties.

Organic fluorophores such as rhodamine or carbocyanine dyes are substantially smaller (~1 nm) (Box 1), and in general exhibit a higher fluorescence quantum yield and improved photostability, but require a chemical labeling procedure. For fixed cells, immunofluorescence is the method of choice using primary and secondary antibodies. The drawback, however, is the size of the commonly used immunoglobulin G antibodies (~10 nm) (Weber et al., 1978) (Box 1), which can deteriorate epitope recognition and increase the apparent size of the actual structure. To reduce the size of the label, direct labeling of the primary antibody or the use of very small labeled camelid antibodies (nanobodies) directed against green fluorescent protein (GFP) (Ries et al., 2012) can be used. Anti-GFP nanobodies have a molecular mass of 13 kDa and a size of 1.5×2.5 nm. Fluorophore-labeled phalloidin, a bi-cyclic heptapeptide from the death cap, and paclitaxel, a drug of the class of taxanes synthesized by fungi in the bark of Pacific yew trees, are very small and efficient labels for the specific labeling of actin and microtubulin filaments, respectively, in fixed cells (Box 1).

Live-cell localization microscopy with organic fluorophores is more demanding, requiring a method for specific and stoichiometric labeling of proteins in living cells with organic fluorophores that can be switched between an on- and off-state in the cellular redox environment. Because living cells naturally contain the reducing glutathione disulfide–glutathione couple (GSH–GSSG) at millimolar concentrations in the cytosol,

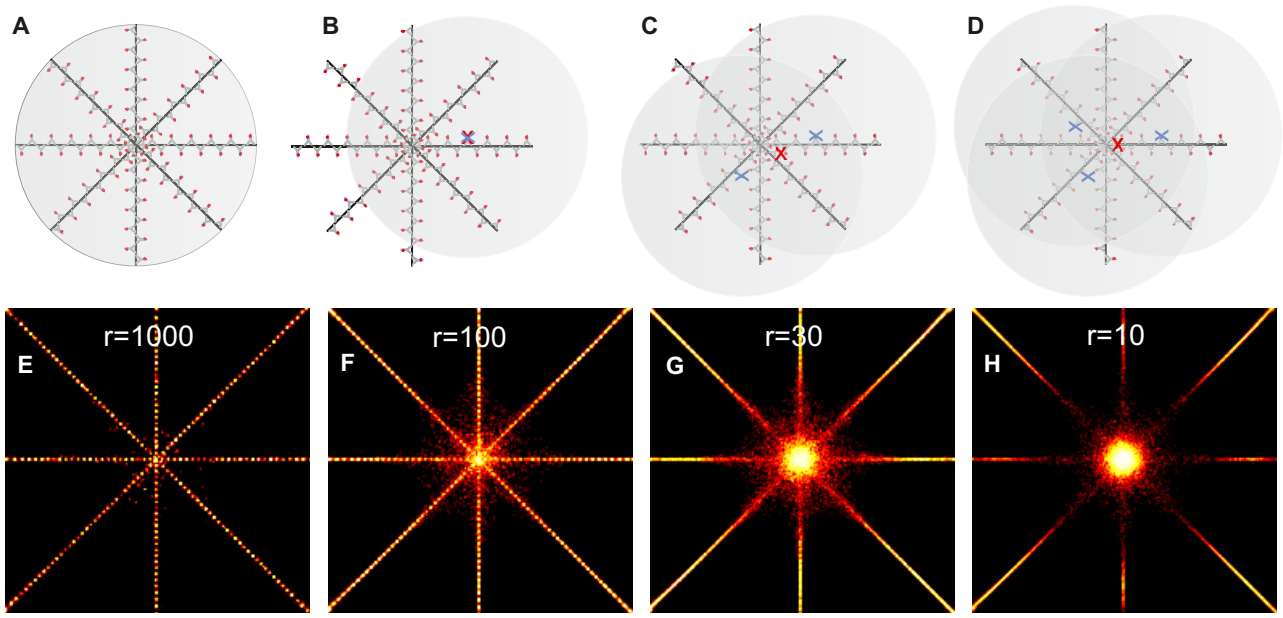

Fig. 1. The effect of photoswitching kinetics and labeling densities on localization microscopy. (**A**) Crossing filaments are labeled with fluorophore-labeled primary antibodies. Every filament consists of a line labeled with antibodies. The circle surrounding the filaments has a diameter of 250 nm, corresponding approximately to the full-weight half maximum (FWHM) of a PSF detected for a single emitting fluorophore. From all antibodies (assuming a degree of labeling of approximately 1) residing in the PSF area, only one can be fluorescent at any time during the experiment in order to generate regular localizations (i.e. localizations that represent the actual position of fluorophores on the structure; see the 'X' on the diagram) (**B**). If two (**C**) or more (**D**) fluorophores reside simultaneously in the on-state, the approximation of the PSF of multiple emitters yields a false position (red X) that does not correspond to the regular physical position (blue X). Such overlapping multiple-fluorophore PSFs result in false localizations and affect the ability to resolve independent filaments. (**E–H**) Simulation of the ability to resolve crossing filaments (2×2 µm per image) labeled with a fluorophore every 40 nm at different photoswitching ratios ($r=k_{off}/k_{on}$). Only for a high photoswitching ratio of r=1000 (e.g. the fluorophores stay on average for 1 ms in the on-state and 1 s in the off-state) is the crossing point clearly resolved. For lower ratios (e.g. r=10–30), false localizations affect the presence of a fluorophore aggregate or cluster (F). Details of data simulations have been described previously (van de Linde et al., 2010). Super-resolved images were reconstructed using rapid*STORM (Wolter et al., 2012).

localization microscopy by *d*STORM is feasible with many Alexa Fluor and ATTO dyes (van de Linde et al., 2011a; van de Linde et al., 2012; van de Linde et al., 2013; Wombacher et al., 2010; Klein et al., 2011; Jones et al., 2011). Post-translational labeling of proteins in living cells can be achieved using genetically encoded polypeptide tags in combination with organic fluorophore ligands (Miller and Cornish, 2005; Fernández-Suárez and Ting, 2008). However, most of these methods still use large protein tags comparable to the size of fluorescent proteins that can sterically interfere with protein function, such as the HaloTag with a molecular mass of 35 kDa (Los et al., 2008), SNAP/CLIP-tags with a molecular mass of 20 kDa (Gautier et al., 2008) and the DHFR/TMP tag with a molecular mass of 18 kDa (Gallagher et al., 2009) (Box 1). So far, different combinations of SNAP-, Halo-, TMP-, CLIP-tags and organic fluorophores have also been successfully used in combination with photoactivatable fluorescent proteins for multi-color live-cell localization microscopy (Appelhans et al., 2012; Benke et al., 2012; Klein et al., 2012; Wilmes et al., 2012). The FlAsH tag, consisting of only 12 amino acids, is much smaller than fluorescent proteins and has been used successfully for intracellular labeling. However, it suffers from problems including labeling specificity and cellular toxicity (Adams et al., 2002; Martin et al., 2005).

Another currently emerging labeling method that is ideally suited for high-density labeling of target structures involves the incorporation of unique chemical functionality into a target molecule using the biosynthesis machinery of the cell (Prescher and Bertozzi, 2005). This so-called bio-orthogonal 'click chemistry' has led to an explosion of interest in the selective covalent labeling of molecules in cells and living organisms (Kolb et al., 2001; Prescher and Bertozzi, 2005; Zessin et al., 2012). Click chemistry relies on a copper-catalyzed azide–alkyne cycloaddition (Box 1). Copper-free alternative labeling methods with improved biocompatibility are also available for live-cell labeling nowadays (Laughlin et al., 2008). Owing to the small size of azide and alkyne tags, modified amino acids, monosaccharides, nucleotides or fatty acids can be metabolically incorporated by living cells or organisms with high efficiency. Finally, the complementary alkyne or azide linked fluorophore are 'clicked' into place. It should be noted that click chemistry, just as any other synthetic labeling method, has the drawback that the labeling efficiency might not be known.

For specific labeling of proteins by click chemistry, a method based on enzyme-catalyzed probe ligation called PRIME (probe incorporation mediated by enzymes) (Uttamapinant et al., 2010) can be used. The central component of the PRIME method is an engineered lipoic acid ligase (LplA) from *Escherichia coli* that catalyzes the covalent tagging of the desired probe to a 13 amino acid recognition sequence called the LplA acceptor peptide (LAP). In the first step, the genetically fused LAP is ligated site-specifically with 10-azidodecanoic acid in cells, and in the second step, fluorophore-modified cyclooctynes react with the azide and form the corresponding aza-dibenzocyclooctyne

Journal of Cell Science

Journal of Cell Science

(ADIBO) (Box 1) (Yao et al., 2012). Alternatively, intracellular proteins can be specifically labeled with, for example, fluorophore-tetrazine derivatives, following the incorporation of genetically encoded unnatural amino acids (UAAs) (Liu and Schultz, 2010).

However, such highly efficient labeling methods can also cause unexpected side effects. With increasing labeling density, the inter-fluorophore distances decrease. Thus, direct electronic quenching interactions between fluorophores, such as in protein aggregates or clusters [e.g. homo-fluorescence resonance energy transfer (homo-FRET) or non-fluorescent fluorophore dimer formation], have to be considered.

Quantification and reliability of localization microcopy

Biological function is often crucially dependent on the quantification of absolute protein numbers in cellular structures or locally in protein complexes such that precise quantification has become increasingly important. Protein numbers are also useful for the generation of quantitative models and simulations, and for the determination of reaction rates in cellular processes. The most direct approach for counting protein molecules is to compare the fluorescence intensity of a protein of interest of a standard with a known protein number labeled with the same fluorophore. Another approach, stepwise photobleaching, relies on stochastic photobleaching of fluorophores upon illumination with light. Whereas quantification by fluorescence intensity is prone to errors owing to fluorescence quenching effects and requires several corrections to achieve accurate measurements (Coffman and Wu, 2012), stepwise photobleaching is limited to low protein numbers because the likelihood of missed events increases exponentially with the number of molecules (Ulbrich and Isacoff, 2007).

Because localization microscopy reconstructs the super-resolved image from single-molecule localization events, it contains information per se about the number of molecules, presupposing that each molecule is labeled with an intact fluorophore, detected above a certain photon threshold and that the number of localizations measured per individual fluorophore is accessible. Naively, one could assume that localization microscopy thus permits direct access to densities and numbers of proteins simply by counting the number of localizations present in time and space, and dividing the total number of localizations by the number of localizations measured for an individual isolated fluorophore under similar experimental conditions.

The first hurdle, however, that has to be overcome is quantitative labeling of the protein of interest. Here, fluorescent proteins offer the distinct advantage of specific stoichiometric labeling of proteins. Unfortunately, fluorescent proteins also show blinking, that is, transient off/on switching that can lead to re-counting of the same fluorophore (Annibale et al., 2010; Annibale et al., 2011; Lando et al., 2012). Strategies to overcome re-counting of fluorescent proteins generally exploit the time dependence of photoswitching of individual fluorophores (Sengupta et al., 2011; Veatch et al., 2012). Another factor that can compromise quantification is that emission from a single fluorophore contributes to more than one image. In addition, problems can arise with the production of stable cell lines expressing endogenous protein levels that show wild-type viability. Furthermore, the fraction of misfolded fluorescent proteins does not always remain negligibly low; even if it did, however, we would not know the percentage of fluorophores missed in the experiment owing to fast photobleaching.

Organic fluorophores are certainly only the second choice for protein quantification because of problems with quantitative labeling and multiple localizations owing to on/off switching on expanded time scales, but they are typically much brighter and more photostable than fluorescent proteins. Thus, the percentage of fluorophores detected and localized accurately is higher. Independent of the fluorophore used, the handling of multiple localizations remains challenging, as it is known that fluorophores change their photophysical properties, including photoswitching performance, depending on their nanoenvironment (Endesfelder et al., 2011). Therefore, isolated fluorophores located outside of the investigated cellular compartment cannot be used as reference. To extract the number of localizations typically detected per fluorophore, it is of utmost importance to perform calibration experiments in the same cellular nanoenvironment with different concentrations of ‘active’ fluorophores. That is, localization microscopy experiments with different concentrations of primary and secondary antibodies (titration experiments) have to be performed to unravel the number of labeled, endogenous proteins.

Yet, the ideal tool to judge the veracity of localization microscopy data is a robust test sample with a well-defined molecular structure and composition. Such test samples can also be used advantageously for calibration of super-resolution imaging instruments and optimization of experimental photoswitching conditions (e.g. irradiation wavelength and intensity, buffer and pH of the solvent). Among the various natural biological samples, the nuclear pore complex (NPC) with its well-defined molecular composition, high density in the nuclear membrane, subdiffraction dimension and eightfold symmetry (Adams and Wente, 2013) holds a special position (Fig. 2) (Löschberger et al., 2012). Thus, the NPC can be used not only to calibrate microscopes, but also to test the achievable resolution of different super-resolution imaging methods by resolving, for example, the central channel of the NPC with a diameter of ~40 nm. Because the NPC is made up of a defined number of proteins, it is also a good test sample for counting the number of molecules in a biological structure. In addition,

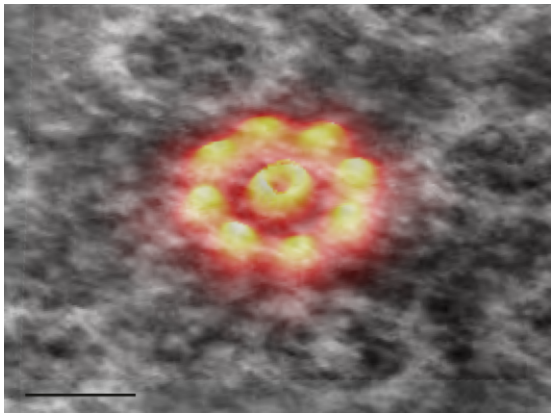

Fig. 2. Superimposed image of accumulated *d*STORM data and an electron microscopy image of the nuclear pore complex. The image demonstrates that localization microscopy and electron microscopy can be used as complementary tools for structural investigations of biomolecular machines (Löschberger et al., 2012). Scale bar: 100 nm.

Journal of Cell Science

centrosomes comprising two orthogonally arranged centrioles, each consisting of nine triplet microtubules (Sillibourne et al., 2011; Lau et al., 2012; Lukinavičius et al., 2013), or pre- and post-synaptic proteins separated by the synaptic cleft (Dani et al., 2010), can also be used as natural biological calibration samples (Box 2). Artificial calibration samples for 2D and 3D localization microscopy include DNA origami (Steinhauer et al., 2009), single-molecule assembled patterns generated by cut-and-paste technology (SMCP) (Kufer et al., 2008; Cordes et al., 2010) and DNA bricks (Box 2) (Ke et al., 2012).

Improving resolution of localization microscopy

Because precision of localization is mainly determined by photon statistics, the collection of more fluorescence photons per switching event is the most important parameter for resolution enhancement. The most direct approach enabling roughly a doubling of the detection efficiency constitutes a dual-objective detection scheme using two opposing objective lenses (Ram et al., 2009; Shtengel et al., 2009; Xu et al., 2012). Alternatively, the photoswitching rates can be decelerated by chemical or physical means, allowing the detection of more fluorescence photons per switching event. Then, however, the increase gained in localization precision is at the cost of the time required to improve the balance between spatial and temporal resolution. In addition, triplet-state quenchers such as cyclooctatetraene (COT) (Altman et al., 2012) can be used to increase the number of fluorescence photons emitted per switching event by optimizing the cycling between the singlet and triplet states before the fluorophore eventually enters a long-lived off-state.

Cooling of the sample to cryogenic temperatures provides the possibility of freezing conformation dynamics and undesired photophysical reactions of fluorophores in the excited state that usually cause photobleaching (Schwartz et al., 2007). Provided that the activation rate of fluorophores can be kept sufficiently low so that only a small subpopulation of spatially well-separated fluorophores resides in the on-state at any time during the experiment, cryo-localization microscopy can potentially allow the detection of orders of magnitude more fluorescence photons, improving the localization precision, even for fluorescent proteins, towards molecular-length scales.

In order to enable the observation of prolonged fluorescence trajectories from single fluorophores at room temperature, ROXS (reducing and oxidizing system) (Vogelsang et al., 2008; Vogelsang et al., 2010) has been introduced. ROXS efficiently quenches long-lived triplet states of fluorophores that have been identified as the origin of different reversible and irreversible photoreactions. As a generally applicable concept, ROXS quenches the triplet state using, for example, a reducing agent such as ascorbic acid, through formation of a radical anion and repopulates the singlet ground state by oxidizing the radical anion with an electron acceptor (e.g. methylviologen). Depending on the redox properties of the fluorophore, the reducing and oxidizing agents and their concentrations, either reduction or oxidation proceeds first and allows the observation of very long fluorescence trajectories from individual fluorophores uninterrupted by fluorescence intermittencies.

The recipes for efficient preparation of off-states that were introduced all share one similarity: the off-state represents a reduced form of the fluorescent on-state of the fluorophore. Upon irradiation of aqueous solutions of rhodamine, carbocyanine and oxazine dyes at their absorption maxima in the presence of millimolar concentrations of thiols such as β-mercaptoethylamine (MEA), reduced species are formed that absorb at shorter wavelengths (Heilemann et al., 2005; Heilemann et al., 2009; van de Linde et al., 2011a). The generated semi-reduced radical anions and fully reduced leuco-dyes exhibit a surprising stability at room temperature in aqueous solvents and can be efficiently transferred to the on-state by weak irradiation at 405 nm or by purging of the sample with oxygen (van de Linde et al., 2011a; van de Linde et al., 2011b, Schäfer et al., 2013). Alternatively, cyanine and rhodamine dyes can be reduced with sodium borohydride ($NaBH_4$) to form the corresponding fully reduced leuco-dyes [i.e. hydrocyanines (Kundu et al., 2009; Vogelsang et al., 2010) and dihydrorhodamines (Edman and Rigler, 2000)] that are commercially available as fluorescent sensors for the detection of reactive oxygen species (ROS) or oxidizing enzymes, respectively.

Therefore, in order to perform localization microscopy with improved resolution at room temperature, the molecule of interest must be first efficiently labeled with a suitable standard fluorophore (Fig. 3). In the second step, the fluorophores are stably reduced. Before a strong reducer such as $NaBH_4$ is used, the structure should be preserved (cross-linked) to minimize artifacts. After generation of stable, fully reduced leuco-dyes, the reducing medium is exchanged with a ROXS buffer containing an oxygen scavenger to minimize auto-oxidation, and reducing and oxidizing substances (e.g. ascorbic acid and methylviologen) (Vogelsang et al., 2008). Importantly, the ROXS buffer has to be designed for cycling the fluorophore through a ROXS-induced radical state that is different from the fully reduced state (leuco-dye) generated by the strong reducer (e.g. $NaBH_4$), such that the fully reduced fluorophores will not be reactivated by the ROXS buffer alone. Finally, ROXS-based localization microcopy is initiated by activation of a sparse subset of reduced fluorophores through irradiation of the sample at 405 nm with low intensity, followed by photobleaching of individual activated fluorophores after detection of several thousand photons. The procedure is repeated until a super-resolved localization microscopy image can be reconstructed. The quality and also the reliability of the resulting super-resolution image is thus mainly determined by the stability of the reduced fluorophores to auto-oxidation and the reversibility of the reducing (or light-induced) oxidizing cycle – that is, the likelihood of irreversible follow-up reactions of the reduced fluorophore.

The first successful demonstration of ROXS-based localization microscopy achieved resolutions of several nanometers, detecting 10^4–10^6 photons per localization (Vaughan et al., 2012). The recovery fraction was 66% for the blue dye ATTO 488, 35–40% for the yellow dyes Cy3 and Cy3B, and 12–17% for the red dyes Alexa 647 and Cy5.5. Besides the use of standard fluorophores that need to be reduced after labeling of the molecule of interest, so-called caged, non-fluorescent dyes that can be activated upon irradiation with UV light, such as rhodamine NN dyes, which have a 2-diazoketone (COCNN) caging group incorporated into a spiro-9H-xanthene fragment (Belov et al., 2010), could also be used for ROXS-based localization microscopy.

The practicality of cryo- or ROXS-based localization microscopy for structural resolution enhancement in biological samples thus crucially relies on two requirements: ultrahigh-density labeling methods to meet the Nyquist criterion; and efficient preparation of fluorophores in stable off-states with the possibility to recover only a small subpopulation to the

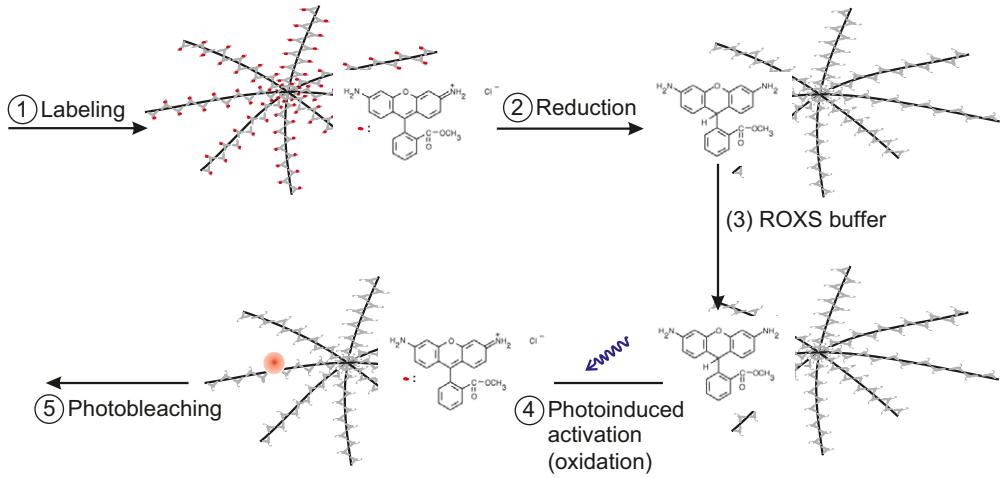

Fig. 3. Schematic principle of ROXS-based localization microscopy with improved optical resolution. Crossing filaments are labeled with fluorophore-labeled primary antibodies. Every filament consists of a line labeled with antibodies. (Step 1) First the molecule of interest is labeled with fluorophores, followed by a cross-linking step with glutaraldehyde to stabilize the structure. (Step 2) The fluorophores are reduced with $NaBH_4$, for example, or other reducers, before the reducing medium is exchanged for a ROXS buffer (Step 3) (Vogelsang et al., 2008). (Step 4) Controlled photoinduced activation of only a subset of reduced fluorophores succeeds upon irradiation with 405 nm light at low intensities (van de Linde et al., 2011a; van de Linde et al., 2011b; Vaughan et al., 2012). (Step 5) Activated (oxidized) fluorophores show long fluorescence trajectories (i.e. they exhibit a much higher photostability) under ROXS buffer conditions providing more photons for their precise localization. The localization precision and structural resolution (presuming that the labeling density is high enough) can be controlled by the photostability of the fluorophores (i.e. the efficiency of the ROXS buffer) by varying, for example, the concentration of the reducing and oxidizing agents.

on-state by external means. Having ultrahigh-density labeling methods at hand (e.g. click chemistry) means the structural resolution could effectively be improved towards achieving the FRET regime of a few nanometers. How such high fluorophore densities affect the blinking properties of fluorophores remains to be studied in future experiments. However, even with scarce label distributions, localization microscopy of multiprotein complexes – so-called molecular machines or nanomachines, such as ribosomes or proteasomes – could be achieved with molecular resolution when the results of multiple inefficient random labeling experiments are combined.

Conclusions

At present, electron microscopy is the gold standard for the investigation of cellular structures at the molecular level. However, far-field fluorescence microscopy methods are catching up quickly, allowing us first insights into the dynamic structural organization of cells and even living organisms at the nanoscale (Berning et al., 2012; Gao et al., 2012). The achievable optical resolution will undoubtedly further increase, thus bridging the gap with the FRET regime and opening new windows for combined FRET and localization microscopy studies (Uphoff et al., 2010). Localization microscopy can also advance the interpretation of fluorescence colocalization microscopy data because it provides single-molecule coordinates rather than intensity information.

Furthermore, localization microscopy is the ideal complementary tool for correlative light and electron microscopy. Whereas electron microscopy can image the cellular context with molecular resolution, localization microscopy can provide quantitative information about distributions and compositions of specifically labeled cellular molecules and machines (Fig. 2). The correlation of function and nanostructural organization (e.g. in synaptic proteins) can likewise be unraveled by combining electrophysiological recording and localization microscopy.

3D localization microscopy based on PSF re-modeling by astigmatism, biplane or more complex approaches is very powerful, but is restricted to thin samples close to the coverslip because refractive index mismatches deteriorate the PSF with increasing axial depth, and thus complicate the determination of the precise axial position. It is not yet possible to accurately answer the question of whether we will soon be able to accomplish 3D whole organism localization microscopy with virtually molecular resolution. Furthermore, imaging entire living organisms involves trade-offs between resolution, speed and phototoxicity. In response to these challenges, both experimental and theoretical improvements are urgently needed to achieve the required balance.

Acknowledgements

The author thanks Sebastian van de Linde for technical assistance and data simulations as well as Sören Doose for careful reading and discussion of the manuscript.

Funding

This work was supported by the Biophotonics Initiative of the Bundesministerium für Bildung und Forschung [grant numbers 13N11019 and 13N12507 to M.S.] and the Deutsche Forschungsgemeinschaft [grant number DFG SA829/8-1 to M.S.].

References

Abbe, E. (1873). Contributions to the theory of the microscope and microscopic detection (translated from German). *Arch. Mikroskop. Anat.* **9**, 413-418.

Adams, R. L. and Wente, S. R. (2013). Uncovering nuclear pore complexity with innovation. *Cell* **152**, 1218-1221.

Adams, S. R., Campbell, R. E., Gross, L. A., Martin, B. R., Walkup, G. K., Yao, Y., Llopis, J. L. and Tsien, R. Y. (2002). New biarsenical ligands and tetracysteine motifs for protein labeling in vitro and in vivo: synthesis and biological applications. *J. Am. Chem. Soc.* **124**, 6063-6076.

Altman, R. B., Terry, D. S., Zhou, Z., Zheng, Q., Geggier, P., Kolster, R. A., Zhao, Y., Javitch, J. A., Warren, J. D. and Blanchard, S. C. (2012). Cyanine fluorophore derivatives with enhanced photostability. *Nat. Methods* **9**, 68-71.

Ando, R., Hama, H., Yamamoto-Hino, M., Mizuno, H. and Miyawaki, A. (2002). An optical marker based on the UV-induced green-to-red photoconversion of a fluorescent protein. *Proc. Natl. Acad. Sci. USA* **99**, 12651-12656.

Annibale, P., Scarselli, M., Kodiyan, A. and Radenovic, A. (2010). Photoactivatable fluorescent protein mEos2 displays repeated photoactivation after a long-lived dark state in the red photoconverted form. *J. Phys. Chem. Lett* **1**, 1506-1510.

Annibale, P., Vanni, S., Scarselli, M., Rothlisberger, U. and Radenovic, A. (2011). Quantitative photo activated localization microscopy: unraveling the effects of photoblinking. *PLoS ONE* **6**, e22678.

Appelhans, T., Richter, C. P., Wilkens, V., Hess, S. T., Piehler, J. and Busch, K. B. (2012). Nanoscale organization of mitochondrial microcompartments revealed by combining tracking and localization microscopy. *Nano Lett.* **12**, 610-616.

Bates, M., Blosser, T. R. and Zhuang, X. W. (2005). Short-range spectroscopic ruler based on a single-molecule optical switch. *Phys. Rev. Lett.* **94**, 108101.

Bates, M., Huang, B., Dempsey, G. T. and Zhuang, X. W. (2007). Multicolor super-resolution imaging with photo-switchable fluorescent probes. *Science* **317**, 1749-1753.

Beck, M., Lucić, V., Förster, F., Baumeister, W. and Medalia, O. (2007). Snapshots of nuclear pore complexes in action captured by cryo-electron tomography. *Nature* **449**, 611-615.

Belov, V. N., Wurm, C. A., Boyarskiy, V. P., Jakobs, S. and Hell, S. W. (2010). Rhodamines NN: a novel class of caged fluorescent dyes. *Angew. Chem. Int. Ed. Engl.* **49**, 3520-3523.

Benke, A., Olivier, N., Gunzenhauser, J. and Manley, S. (2012). Multicolor single molecule tracking of stochastically active synthetic dyes. *Nano Lett.* **12**, 2619-2624.

Berning, S., Willig, K. I., Steffens, H., Dibaj, P. and Hell, S. W. (2012). Nanoscopy in a living mouse brain. *Science* **335**, 551.

Betzig, E., Patterson, G. H., Sougrat, R., Lindwasser, O. W., Olenych, S., Bonifacino, J. S., Davidson, M. W., Lippincott-Schwartz, J. and Hess, H. F. (2006). Imaging intracellular fluorescent proteins at nanometer resolution. *Science* **313**, 1642-1645.

Coffman, V. C. and Wu, J.-Q. (2012). Counting protein molecules using quantitative fluorescence microscopy. *Trends Biochem. Sci.* **37**, 499-506.

Cordes, T., Strackharn, M., Stahl, S. W., Summerer, W., Steinhauer, C., Forthmann, C., Puchner, E. M., Vogelsang, J., Gaub, H. E. and Tinnefeld, P. (2010). Resolving single-molecule assembled patterns with superresolution blink-microscopy. *Nano Lett.* **10**, 645-651.

Dani, A., Huang, B., Bergan, J., Dulac, C. and Zhuang, X. (2010). Superresolution imaging of chemical synapses in the brain. *Neuron* **68**, 843-856.

Dempsey, G. T., Vaughan, J. C., Chen, K. H., Bates, M. and Zhuang, X. (2011). Evaluation of fluorophores for optimal performance in localization-based super-resolution imaging. *Nat. Methods* **8**, 1027-1036.

Dickson, R. M., Cubitt, A. B., Tsien, R. Y. and Moerner, W. E. (1997). On/off blinking and switching behaviour of single molecules of green fluorescent protein. *Nature* **388**, 355-358.

Edman, L. and Rigler, R. (2000). Memory landscapes of single-enzyme molecules. *Proc. Natl. Acad. Sci. USA* **97**, 8266-8271.

Endesfelder, U., Malkusch, S., Flottmann, B., Mondry, J., Liguzinski, P., Verveer, P. J. and Heilemann, M. (2011). Chemically induced photoswitching of fluorescent probes—a general concept for super-resolution microscopy. *Molecules* **16**, 3106-3118.

Fernández-Suárez, M. and Ting, A. Y. (2008). Fluorescent probes for super-resolution imaging in living cells. *Nat. Rev. Mol. Cell Biol.* **9**, 929-943.

Fölling, J., Bossi, M., Bock, H., Medda, R., Wurm, C. A., Hein, B., Jakobs, S., Eggeling, C. and Hell, S. W. (2008). Fluorescence nanoscopy by ground-state depletion and single-molecule return. *Nat. Methods* **5**, 943-945.

Galbraith, C. G. and Galbraith, J. A. (2011). Super-resolution microscopy at a glance. *J. Cell Sci.* **124**, 1607-1611.

Gallagher, S. S., Sable, J. E., Sheetz, M. P. and Cornish, V. W. (2009). An in vivo covalent TMP-tag based on proximity-induced reactivity. *ACS Chem. Biol.* **4**, 547-556.

Gao, L., Shao, L., Higgins, C. D., Poulton, J. S., Peifer, M., Davidson, M. W., Wu, X., Goldstein, B. and Betzig, E. (2012). Noninvasive imaging beyond the diffraction limit of 3D dynamics in thickly fluorescent specimens. *Cell* **151**, 1370-1385.

Gautier, A., Juillerat, A., Heinis, C., Corrêa, I. R., Jr, Kindermann, M., Beaufils, F. and Johnsson, K. (2008). An engineered protein tag for multiprotein labeling in living cells. *Chem. Biol.* **15**, 128-136.

Giannone, G., Hosy, E., Levet, F., Constals, A., Schulze, K., Sobolevsky, A. I., Rosconi, M. P., Gouaux, E., Tampé, R., Choquet, D. et al. (2010). Dynamic superresolution imaging of endogenous proteins on living cells at ultra-high density. *Biophys. J.* **99**, 1303-1310.

Heilemann, M., Herten, D. P., Heintzmann, R., Cremer, C., Müller, C., Tinnefeld, P., Weston, K. D., Wolfrum, J. and Sauer, M. (2002). High-resolution colocalization of single dye molecules by fluorescence lifetime imaging microscopy. *Anal. Chem.* **74**, 3511-3517.

Heilemann, M., Margeat, E., Kasper, R., Sauer, M. and Tinnefeld, P. (2005). Carbocyanine dyes as efficient reversible single-molecule optical switch. *J. Am. Chem. Soc.* **127**, 3801-3806.

Heilemann, M., van de Linde, S., Schüttpelz, M., Kasper, R., Seefeldt, B., Mukherjee, A., Tinnefeld, P. and Sauer, M. (2008). Subdiffraction-resolution fluorescence imaging with conventional fluorescent probes. *Angew. Chem. Int. Ed. Engl.* **47**, 6172-6176.

Heilemann, M., van de Linde, S., Mukherjee, A. and Sauer, M. (2009). Superresolution imaging with small organic fluorophores. *Angew. Chem. Int. Ed.* **48**, 6903-6908.

Hell, S. W. (2007). Far-field optical nanoscopy. *Science* **316**, 1153-1158.

Hess, S. T., Girirajan, T. P. and Mason, M. D. (2006). Ultra-high resolution imaging by fluorescence photoactivation localization microscopy. *Biophys. J.* **91**, 4258-4272.

Hess, S. T., Gould, T. J., Gudheti, M. V., Maas, S. A., Mills, K. D. and Zimmerberg, J. (2007). Dynamic clustered distribution of hemagglutinin resolved at 40 nm in living cell membranes discriminates between raft theories. *Proc. Natl. Acad. Sci. USA* **104**, 17370-17375.

Holden, S. J., Uphoff, S. and Kapanidis, A. N. (2011). DAOSTORM: an algorithm for high- density super-resolution microscopy. *Nat. Methods* **8**, 279-280.

Jones, S. A., Shim, S. H., He, J. and Zhuang, X. (2011). Fast, three-dimensional super-resolution imaging of live cells. *Nat. Methods* **8**, 499-508.

Kaminski Schierle, G. S., van de Linde, S., Erdelyi, M., Esbjörner, E. K., Klein, T., Rees, E., Bertoncini, C. W., Dobson, C. M., Sauer, M. and Kaminski, C. F. (2011). In situ measurements of the formation and morphology of intracellular β-amyloid fibrils by super-resolution fluorescence imaging. *J. Am. Chem. Soc.* **133**, 12902-12905.

Kanchanawong, P., Shtengel, G., Pasapera, A. M., Ramko, E. B., Davidson, M. W., Hess, H. F. and Waterman, C. M. (2010). Nanoscale architecture of integrin-based cell adhesions. *Nature* **468**, 580-584.

Ke, Y., Ong, L. L., Shih, W. M. and Yin, P. (2012). Three-dimensional structures self-assembled from DNA bricks. *Science* **338**, 1177-1183.

Kitagawa, D., Vakonakis, I., Olieric, N., Hilbert, M., Keller, D., Olieric, V., Bortfeld, M., Erat, M. C., Flückiger, I., Gönczy, P. et al. (2011). Structural basis of the 9-fold symmetry of centrioles. *Cell* **144**, 364-375.

Klein, T., Löschberger, A., Proppert, S., Wolter, S., van de Linde, S. and Sauer, M. (2011). Live-cell *d*STORM with SNAP-tag fusion proteins. *Nat. Methods* **8**, 7-9.

Klein, T., van de Linde, S. and Sauer, M. (2012). Live-cell super-resolution imaging goes multicolor. *Chembiochem.* **13**, 1861-1863.

Kolb, H. C., Finn, M. G. and Sharpless, K. B. (2001). Click Chemistry: Diverse Chemical Function from a Few Good Reactions. *Angew. Chem. Int. Ed. Engl.* **40**, 2004-2021.

Kufer, S. K., Puchner, E. M., Gumpp, H., Liedl, T. and Gaub, H. E. (2008). Single-molecule cut-and-paste surface assembly. *Science* **319**, 594-596.

Kundu, K., Knight, S. F., Willett, N., Lee, S., Taylor, W. R. and Murthy, N. (2009). Hydrocyanines: a class of fluorescent sensors that can image reactive oxygen species in cell culture, tissue, and in vivo. *Angew. Chem. Int. Ed. Engl.* **48**, 299-303.

Lacoste, T. D., Michalet, X., Pinaud, F., Chemla, D. S., Alivisatos, A. P. and Weiss, S. (2000). Ultrahigh-resolution multicolor colocalization of single fluorescent probes. *Proc. Natl. Acad. Sci. USA* **97**, 9461-9466.

Lampe, A., Haucke, V., Sigrist, S. J., Heilemann, M. and Schmoranzer, J. (2012). Multi-colour direct STORM with red emitting carbocyanines. *Biol. Cell* **104**, 229-237.

Lando, D., Endesfelder, U., Berger, H., Subramanian, L., Dunne, P. D., McColl, J., Klenerman, D., Carr, A. M., Sauer, M., Allshire, R. C. et al. (2012). Quantitative single-molecule microscopy reveals that CENP-A(Cnp1) deposition occurs during G2 in fission yeast. *Open Biol.* **2**, 120078.

Lau, L., Lee, Y. L., Sahl, S. J., Stearns, T. and Moerner, W. E. (2012). STED microscopy with optimized labeling density reveals 9-fold arrangement of a centriole protein. *Biophys. J.* **102**, 2926-2935.

Laughlin, S. T., Baskin, J. M., Amacher, S. L. and Bertozzi, C. R. (2008). In vivo imaging of membrane-associated glycans in developing zebrafish. *Science* **320**, 664-667.

Lidke, K., Rieger, B., Jovin, T. and Heintzmann, R. (2005). Superresolution by localization of quantum dots using blinking statistics. *Opt. Express* **13**, 7052-7062.

Lippincott-Schwartz, J. and Patterson, G. H. (2009). Photoactivatable fluorescent proteins for diffraction-limited and super-resolution imaging. *Trends Cell Biol.* **19**, 555-565.

Liu, C. C. and Schultz, P. G. (2010). Adding new chemistries to the genetic code. *Annu. Rev. Biochem.* **79**, 413-444.

Los, G. V., Encell, L. P., McDougall, M. G., Hartzell, D. D., Karassina, N., Zimprich, C., Wood, M. G., Learish, R., Ohana, R. F., Urh, M. et al. (2008). HaloTag: a novel protein labeling technology for cell imaging and protein analysis. *ACS Chem. Biol.* **3**, 373-382.

Löschberger, A., van de Linde, S., Dabauvalle, M. C., Rieger, B., Heilemann, M., Krohne, G. and Sauer, M. (2012). Super-resolution imaging visualizes the eightfold symmetry of gp210 proteins around the nuclear pore complex and resolves the central channel with nanometer resolution. *J. Cell Sci.* **125**, 570-575.

Lukinavičius, G., Umezawa, K., Olivier, N., Honigmann, A., Yang, G., Plass, T., Mueller, V., Reymond, L., Corrêa, I. R., Jr, Luo, Z.-G. et al. (2013). A near-infrared fluorophore for live-cell super-resolution microscopy of cellular proteins. *Nat. Chem.* **5**, 132-139.

Manley, S., Gillette, J. M., Patterson, G. H., Shroff, H., Hess, H. F., Betzig, E. and Lippincott-Schwartz, J. (2008). High-density mapping of single-molecule trajectories with photoactivated localization microscopy. *Nat. Methods* **5**, 155-157.

Martin, B. R., Giepmans, B. N., Adams, S. R. and Tsien, R. Y. (2005). Mammalian cell-based optimization of the biarsenical-binding tetracysteine motif for improved fluorescence and affinity. *Nat. Biotechnol.* **23**, 1308-1314.

Mattila, P. K., Feest, C., Depoil, D., Treanor, B., Montaner, B., Otipoby, K. L., Carter, R., Justement, L. B., Bruckbauer, A. and Batista, F. D. (2013). The actin and tetraspanin networks organize receptor nanoclusters to regulate B cell receptor-mediated signaling. *Immunity* **38**, 461-474.

Miller, L. W. and Cornish, V. W. (2005). Selective chemical labeling of proteins in living cells. *Curr. Opin. Chem. Biol.* **9**, 56-61.

Journal of Cell Science

Moerner, W. E. and Orrit, M. (1999). Illuminating single molecules in condensed matter. *Science* **283**, 1670-1676.
Mortensen, K. I., Churchman, L. S., Spudich, J. A. and Flyvbjerg, H. (2010). Optimized localization analysis for single-molecule tracking and super-resolution microscopy. *Nat. Methods* **1**, 377-381.
Ormö, M., Cubitt, A. B., Kallio, K., Gross, L. A., Tsien, R. Y. and Remington, S. J. (1996). Crystal structure of the Aequorea victoria green fluorescent protein. *Science* **273**, 1392-1395.
Patterson, G. H. and Lippincott-Schwartz, J. (2002). A photoactivatable GFP for selective photolabeling of proteins and cells. *Science* **297**, 1873-1877.
Pertsinidis, A., Zhang, Y. and Chu, S. (2010). Subnanometre single-molecule localization, registration and distance measurements. *Nature* **466**, 647-651.
Prescher, J. A. and Bertozzi, C. R. (2005). Chemistry in living systems. *Nat. Chem. Biol.* **1**, 13-21.
Ram, S., Prabhat, P., Ward, E. S. and Ober, R. J. (2009). Improved single particle localization accuracy with dual objective multifocal plane microscopy. *Opt. Express* **17**, 6881-6898.
Ribrault, C., Sekimoto, K. and Triller, A. (2011). From the stochasticity of molecular processes to the variability of synaptic transmission. *Nat. Rev. Neurosci.* **12**, 375-387.
Ries, J., Kaplan, C., Platonova, E., Eghlidi, H. and Ewers, H. (2012). A simple, versatile method for GFP-based super-resolution microscopy via nanobodies. *Nat. Methods* **9**, 582-584.
Roeffaers, M. B., De Cremer, G., Libeert, J., Ameloot, R., Dedecker, P., Bons, A. J., Bückins, M., Martens, J. A., Sels, B. F., De Vos, D. E. et al. (2009). Super-resolution reactivity mapping of nanostructured catalyst particles. *Angew. Chem. Int. Ed. Engl.* **48**, 9285-9289.
Rossy, J., Owen, D. M., Williamson, D. J., Yang, Z. and Gaus, K. (2013). Conformational states of the kinase Lck regulate clustering in early T cell signaling. *Nat. Immunol.* **14**, 82-89.
Rothemund, P. W. (2006). Folding DNA to create nanoscale shapes and patterns. *Nature* **440**, 297-302.
Rust, M. J., Bates, M. and Zhuang, X. W. (2006). Sub-diffraction-limit imaging by stochastic optical reconstruction microscopy (STORM). *Nat. Methods* **3**, 793-795.
Saccà, B. and Niemeyer, C. M. (2012). DNA origami: the art of folding DNA. *Angew. Chem. Int. Ed. Engl.* **51**, 58-66.
Schäfer, P., van de Linde, S., Lehmann, J., Sauer, M. and Doose, S. (2013). Methylene blue- and thiol-based oxygen depletion for super-resolution imaging. *Anal. Chem.* **85**, 3393-3400.
Schwartz, C. L., Sarbash, V. I., Ataullakhanov, F. I., McIntosh, J. R. and Nicastro, D. (2007). Cryo-fluorescence microscopy facilitates correlations between light and cryo-electron microscopy and reduces the rate of photobleaching. *J. Microsc.* **227**, 98-109.
Sengupta, P., Jovanovic-Talisman, T., Skoko, D., Renz, M., Veatch, S. L. and Lippincott-Schwartz, J. (2011). Probing protein heterogeneity in the plasma membrane using PALM and pair correlation analysis. *Nat. Methods* **8**, 969-975.
Shannon, C. E. (1949) Communication in the presence of noise. *Proc. IEEE Inst. Electr. Electron Eng.* **37**, 10-21.
Sharonov, A. and Hochstrasser, R. M. (2006). Wide-field subdiffraction imaging by accumulated binding of diffusing probes. *Proc. Natl. Acad. Sci. USA* **103**, 18911-18916.
Shroff, H., Galbraith, C. G., Galbraith, J. A., White, H., Gillette, J., Olenych, S., Davidson, M. W. and Betzig, E. (2007). Dual-color superresolution imaging of genetically expressed probes within individual adhesion complexes. *Proc. Natl. Acad. Sci. USA* **104**, 20308-20313.
Shroff, H., Galbraith, C. G., Galbraith, J. A. and Betzig, E. (2008). Live-cell photoactivated localization microscopy of nanoscale adhesion dynamics. *Nat. Methods* **5**, 417-423.
Shtengel, G., Galbraith, J. A., Galbraith, C. G., Lippincott-Schwartz, J., Gillette, J. M., Manley, S., Sougrat, R., Waterman, C. M., Kanchanawong, P., Davidson, M. W. et al. (2009). Interferometric fluorescent super-resolution microscopy resolves 3D cellular ultrastructure. *Proc. Natl. Acad. Sci. USA* **106**, 3125-3130.
Sillibourne, J. E., Specht, C. G., Izeddin, I., Hurbain, I., Tran, P., Triller, A., Darzacq, X., Dahan, M. and Bornens, M. (2011). Assessing the localization of centrosomal proteins by PALM/STORM nanoscopy. *Cytoskeleton* **68**, 619-627.
Steinhauer, C., Forthmann, C., Vogelsang, J. and Tinnefeld, P. (2008). Superresolution microscopy on the basis of engineered dark states. *J. Am. Chem. Soc.* **130**, 16840-16841.
Steinhauer, C., Jungmann, R., Sobey, T. L., Simmel, F. C. and Tinnefeld, P. (2009). DNA origami as a nanoscopic ruler for super-resolution microscopy. *Angew. Chem. Int. Ed. Engl.* **48**, 8870-8873.
Subach, F. V., Patterson, G. H., Manley, S., Gillette, J. M., Lippincott-Schwartz, J. and Verkhusha, V. V. (2009). Photoactivatable mCherry for high-resolution two-color fluorescence microscopy. *Nat. Methods* **6**, 153-159.
Thompson, R. E., Larson, D. R. and Webb, W. W. (2002). Precise nanometer localization analysis for individual fluorescent probes. *Biophys. J.* **82**, 2775-2783.
Tinnefeld, P. and Sauer, M. (2005). Branching out of single-molecule fluorescence spectroscopy: challenges for chemistry and influence on biology. *Angew. Chem. Int. Ed. Engl.* **44**, 2642-2671.
Tørring, T., Voigt, N. V., Nangreave, J., Yan, H. and Gothelf, K. V. (2011). DNA origami: a quantum leap for self-assembly of complex structures. *Chem. Soc. Rev.* **40**, 5636-5646.
Tsien, R. Y. (1998). The green fluorescent protein. *Annu. Rev. Biochem.* **67**, 509-544.
Ulbrich, M. H. and Isacoff, E. Y. (2007). Subunit counting in membrane-bound proteins. *Nat. Methods* **4**, 319-321.
Uphoff, S., Holden, S. J., Le Reste, L., Periz, J., van de Linde, S., Heilemann, M. and Kapanidis, A. N. (2010). Monitoring multiple distances within a single molecule using switchable FRET. *Nat. Methods* **7**, 831-836.
Uttamapinant, C., White, K. A., Baruah, H., Thompson, S., Fernández-Suárez, M., Puthenveetil, S. and Ting, A. Y. (2010). A fluorophore ligase for site-specific protein labeling inside living cells. *Proc. Natl. Acad. Sci. USA* **107**, 10914-10919.
van de Linde, S., Wolter, S., Heilemann, M. and Sauer, M. (2010). The effect of photoswitching kinetics and labeling densities on super-resolution fluorescence imaging. *J. Biotechnol.* **149**, 260-266.
van de Linde, S., Löschberger, A., Klein, T., Heidbreder, M., Wolter, S., Heilemann, M. and Sauer, M. (2011a). Direct stochastic optical reconstruction microscopy with standard fluorescent probes. *Nat. Protoc.* **6**, 991-1009.
van de Linde, S., Krstić, I., Prisner, T., Doose, S., Heilemann, M. and Sauer, M. (2011b). Photoinduced formation of reversible dye radicals and their impact on super-resolution imaging. *Photochem. Photobiol. Sci.* **10**, 499-506.
van de Linde, S., Heilemann, M. and Sauer, M. (2012). Live-cell super-resolution imaging with synthetic fluorophores. *Annu. Rev. Phys. Chem.* **63**, 519-540.
van de Linde, S., Aufmkolk, S., Franke, C., Holm, T., Klein, T., Löschberger, A., Proppert, S., Wolter, S. and Sauer, M. (2013). Investigating cellular structures at the nanoscale with organic fluorophores. *Chem. Biol.* **20**, 8-18.
Vaughan, J. C., Jia, S. and Zhuang, X. (2012). Ultrabright photoactivatable fluorophores created by reductive caging. *Nat. Methods* **9**, 1181-1184.
Veatch, S. L., Machta, B. B., Shelby, S. A., Chiang, E. N., Holowka, D. A. and Baird, B. A. (2012). Correlation functions quantify super-resolution images and estimate apparent clustering due to over-counting. *PLoS ONE* **7**, e31457.
Vogelsang, J., Kasper, R., Steinhauer, C., Person, B., Heilemann, M., Sauer, M. and Tinnefeld, P. (2008). A reducing and oxidizing system minimizes photobleaching and blinking of fluorescent dyes. *Angew. Chem. Int. Ed. Engl.* **47**, 5465-5469.
Vogelsang, J., Steinhauer, C., Forthmann, C., Stein, I. H., Person-Skegro, B., Cordes, T. and Tinnefeld, P. (2010). Make them blink: probes for super-resolution microscopy. *ChemPhysChem* **11**, 2475-2490.
Weber, K., Rathke, P. C. and Osborn, M. (1978). Cytoplasmic microtubular images in glutaraldehyde-fixed tissue culture cells by electron microscopy and by immunofluorescence microscopy. *Proc. Natl. Acad. Sci. USA* **75**, 1820-1824.
Williamson, D. J., Owen, D. M., Rossy, J., Magenau, A., Wehrmann, M., Gooding, J. J. and Gaus, K. (2011). Pre-existing clusters of the adaptor Lat do not participate in early T cell signaling events. *Nat. Immunol.* **12**, 655-662.
Wilmes, S., Staufenbiel, M., Lisse, D., Richter, C. P., Beutel, O., Busch, K. B., Hess, S. T. and Piehler, J. (2012). Triple-color super-resolution imaging of live cells: resolving submicroscopic receptor organization in the plasma membrane. *Angew. Chem. Int. Ed. Engl.* **51**, 4868-4871.
Wolter, S., Schüttpelz, M., Tscherepanow, M., VAN DE Linde, S., Heilemann, M. and Sauer, M. (2010). Real-time computation of subdiffraction-resolution fluorescence images. *J. Microsc.* **237**, 12-22.
Wolter, S., Endesfelder, U., van de Linde, S., Heilemann, M. and Sauer, M. (2011). Measuring localization performance of super-resolution algorithms on very active samples. *Opt. Express* **19**, 7020-7033.
Wolter, S., Löschberger, A., Holm, T., Aufmkolk, S., Dabauvalle, M.-C., van de Linde, S. and Sauer, M. (2012). rapidSTORM: accurate, fast open-source software for localization microscopy. *Nat. Methods* **9**, 1040-1041.
Wombacher, R., Heidbreder, M., van de Linde, S., Sheetz, M. P., Heilemann, M., Cornish, V. W. and Sauer, M. (2010). Live-cell super-resolution imaging with trimethoprim conjugates. *Nat. Methods* **7**, 717-719.
Xu, K., Babcock, H. P. and Zhuang, X. (2012). Dual-objective STORM reveals three-dimensional filament organization in the actin cytoskeleton. *Nat. Methods* **9**, 185-188.
Yao, J. Z., Uttamapinant, C., Poloukhtine, A., Baskin, J. M., Codelli, J. A., Sletten, E. M., Bertozzi, C. R., Popik, V. V. and Ting, A. Y. (2012). Fluorophore targeting to cellular proteins via enzyme-mediated azide ligation and strain-promoted cycloaddition. *J. Am. Chem. Soc.* **134**, 3720-3728.
Yildiz, A. and Selvin, P. R. (2005). Fluorescence imaging with one nanometer accuracy: application to molecular motors. *Acc. Chem. Res.* **38**, 574-582.
Zessin, P. J., Finan, K. and Heilemann, M. (2012). Super-resolution fluorescence imaging of chromosomal DNA. *J. Struct. Biol.* **177**, 344-348.
Zhu, L., Zhang, W., Elnatan, D. and Huang, B. (2012). Faster STORM using compressed sensing. *Nat. Methods* **9**, 721-723.

Journal of Cell Science